Chinese Journal of Natural Medicines

Potential therapeutic benefits of *Murraya exotica* L. extract on type II collagen-induced arthritis

Guoping Wu, Yuxin Fan, Yawen Yao, Qiushuo Ma, Qiling Chen, Junming Chen, Wenbo Xie, Hua Yu

Citation: Guoping Wu, Yuxin Fan, Yawen Yao, Qiushuo Ma, Qiling Chen, Junming Chen, Wenbo Xie, Hua Yu, Potential therapeutic benefits of *Murraya exotica* L. extract on type II collagen-induced arthritis, Chinese Journal of Natural Medicines, 2026, 24(5), 604-618. doi: 10.1016/S1875-5364(26)61179-X.

View online: https://doi.org/10.1016/S1875-5364(26)61179-X

Chinese Journal of Natural Medicines 24 (2026) 604-618

Contents lists available at ScienceDirect

Chinese Journal of Natural Medicines

journal homepage: www.cjnmcpu.com/

Original article

Potential therapeutic benefits of *Murraya exotica* L. extract on type II collagen-induced arthritis

Guoping Wu[a,Δ], Yuxin Fan[a,Δ], Yawen Yao[a], Qiushuo Ma[a], Qiling Chen[a], Junming Chen[a], Wenbo Xie[c], Hua Yu[a,b,*]

[a] *State Key Laboratory of Mechanism and Quality of Chinese Medicine, Institute of Chinese Medical Sciences, University of Macau, Macao 999078, China*
[b] *Macao Centre for Research and Development in Chinese Medicine, Institute of Chinese Medical Sciences, University of Macau, Macao 999078, China*
[c] *China Resources Sanjiu Medical & Pharmaceutical Co., Ltd., Shenzhen 518000, China*

ARTICLE INFO

Article history:
Received 20 October 2025
Revised 23 January 2026
Accepted 10 March 2026
Available online 20 May 2026

Keywords:
Rheumatoid arthritis
Murraya exotica L.
Murrayae Folium et Cacumen
Synovial hyperplasia
Inflammation
Oxidative stress
NF-κB
AP-1

ABSTRACT

Rheumatoid arthritis (RA) is a chronic, progressive autoimmune disorder characterized by persistent synovial inflammation, pannus formation, bone erosion, and eventual joint destruction. *Murraya exotica* L. (ME), a botanical source of Murrayae Folium et Cacumen (MFC), has not been previously investigated for its anti-arthritic potential, which motivated this study. The chemical composition of ME was characterized using ultra-performance liquid chromatography (UPLC), and its anti-arthritic effects were evaluated in collagen-induced arthritis (CIA) rats and interleukin (IL)-1β-stimulated SW982 cells. The contents of meranzin hydrate, hainanmurpanin, murrayone, and 3',4',5,5',6,7-hexamethoxyflavone in the ME extract were quantified as 2.86% ± 0.01%, 1.88% ± 0.01%, 0.07% ± 0.00%, and 0.01% ± 0.00%, respectively. In CIA rats, ME treatment alleviated clinical symptoms, attenuated histopathological joint damage, including synovial hyperplasia, cartilage degeneration, and bone erosion, ameliorated inflammation, and reduced oxidative stress. In IL-1β-stimulated SW982 cells, ME inhibited proliferation and migration, suppressed the inflammatory response, and mitigated oxidative stress. Network pharmacology and molecular docking analyses predicted strong interactions between ME-derived compounds (e.g., murrayone) and nuclear factor-kappa B (NF-κB) p65, which were further validated by cellular thermal shift assay (CETSA) and drug affinity responsive target stability (DARTS) assay. Mechanistically, ME blocked NF-κB activation by inhibiting phosphorylation and degradation of inhibitor of NF-κB-α (IκBα) and preventing p65 nuclear translocation, while simultaneously suppressing activator protein-1 (AP-1) activation through downregulation of c-Fos and c-Jun. The involvement of the NF-κB and AP-1 pathways in ME-mediated anti-inflammatory, anti-proliferative, and anti-oxidative effects in RA was further confirmed using specific pharmacological inhibitors: pyrrolidinedithiocarbamate (PDTC) for NF-κB and SR11302 for AP-1.

1. Introduction

Rheumatoid arthritis (RA), a chronic progressive autoimmune disease affecting approximately 1% of adults globally, is characterized by persistent synovial inflammation, pannus formation, bone erosion, and irreversible joint destruction [1,2]. Current therapeutic approaches, including corticosteroids, non-steroidal anti-inflammatory drugs (NSAIDs), disease-modifying anti-rheumatic drugs (DMARDs), and biologics, primarily aim to alleviate symptoms and delay disease progression; however, their limited efficacy and suboptimal safety profiles underscore the need for alternative therapeutic strategies [3].

Traditional Chinese medicines (TCMs), recognized for their multi-target effects and favorable safety profiles, represent promising therapeutic candidates [4]. Chinese herbal medicines (CHMs), often derived from multiple plant species, reflect historical development patterns and regional therapeutic practices [5]. Murrayae Folium et Cacumen (MFC), a representative multi-sourced CHM, consists of the dried leaves and branches of two aromatic Rutaceae species: *Murraya exotica* L. (ME) and *Murraya paniculata* (L.) Jack (MP). Traditionally, MFC is used to invigorate qi, relieve pain, promote blood circulation, and disperse blood stasis [6], and it is commonly employed in treating gastric pain, rheumatism, joint pain, toothache, swelling, and snake bites [7]. Haizhen Liang et al. identified five coumarin derivatives isolated from the leaves and twigs of ME that exhibited significant anti-inflammatory activity by inhibiting lipopolysaccharide-stimulated nitric oxide production in RAW264.7 macrophages [8]. Isomeranzin, a coumarin extracted from ME, demonstrated potential to ameliorate inflammation by suppressing M1 macrophage polarization through inhibition of nuclear factor-kappa B (NF-κB) and ERK activation [9]. Furthermore, Jishang Huang et al. reported that 5,7,3',4'-tetramethoxyflavone (TMF), a natural flavonoid derived from ME, effectively inhibited chondrocyte hypertrophy in os-

* Corresponding author.
E-mail address: bcalecyu@um.edu.mo (H. Yu)
Δ These authors contributed equally to this work.

https://doi.org/10.1016/S1875-5364(26)61179-X

teoarthritic cartilage by modulating the FOXO3a/BMPER signaling axis, further supporting the therapeutic potential of ME in arthritis treatment [10]. Nevertheless, the precise protective effects and underlying molecular mechanisms of ME in arthritis management remain insufficiently explored, warranting further investigation and highlighting its potential as a complementary therapy for current RA treatments.

The etiology and pathogenesis of RA involve dysregulated interactions among fibroblasts, macrophages, T and B lymphocytes, and osteoclasts [11, 12]. Fibroblast-like synoviocytes (FLSs), key resident cells in the synovium responsible for maintaining synovial fluid homeostasis and regulating the extracellular matrix, undergo pathological transformation into RA-FLSs, which exhibit resistance to apoptosis, aberrant proliferation, and enhanced migratory capacity, ultimately driving invasive pannus formation [13, 14]. Activated FLSs perpetuate inflammation through sustained secretion of pro-inflammatory mediators, including cytokines, chemokines, matrix metalloproteinases (MMPs), and adhesion molecules, thereby exacerbating joint destruction and immune dysregulation [15]. Moreover, numerous studies have established that immune-mediated inflammation and oxidative stress are intricately linked and play pivotal roles in RA pathogenesis [16]. The excessive accumulation of reactive oxygen species (ROS) induces oxidative stress, which acts as a critical amplifier of inflammatory responses [17]. Consequently, FLSs have emerged as essential cellular targets for elucidating RA pathogenesis and developing novel therapeutic interventions.

This study systematically evaluates the anti-arthritic potential of ME in both collagen-induced arthritis (CIA) rats and interleukin (IL)-1β-stimulated SW982 cells, with the aim of elucidating the mechanisms underlying ME's anti-proliferative, anti-inflammatory, and anti-oxidative effects. Network pharmacology is employed to map drug–disease interactions, and molecular docking is used to validate the binding affinity of ME-derived compounds to key molecular targets. These findings are expected to provide theoretical support for the application of ME in RA treatment and offer promising avenues for future therapeutic strategies against this debilitating condition.

2. Materials and methods

2.1. Chemicals and reagents

Meranzin hydrate, hainanmurpanin, murrayone, and 3',4',5,5',6,7-hexamethoxyflavone (all HPLC-confirmed purity ≥ 98%) were provided by Sichuan Weikeqi Biological Technology Co., Ltd. (Sichuan, China). Enzyme-linked immunosorbent assay (ELISA) kits for human tumor necrosis factor (TNF)-α, immunoglobulin G (IgG) and pro-inflammatory cytokines [IL-6, IL-8, IL-1β, and monocyte chemotactic protein (MCP)-1], as well as for rat IgA, IgG, IL-6, IL-17/17A, MCP-1, TNF-α, IL-10, IL-2, and IL-1β quantification, were obtained from Neobioscience Technology Co., Ltd. (Shenzhen, China). Primers for glyceraldehyde-3-phosphate dehydrogenase (GAPDH), TNF-α, IL-6, IL-8, and IL-1β were synthesized by Guangzhou Ige Biotechnology, Ltd. (Guangdong, China). Biochemical biomarkers, including aspartate transaminase (AST), alanine transaminase (ALT), alkaline phosphatase (AKP), γ-glutamyltransferase (γ-GT), creatinine (CRE), and blood urea nitrogen (BUN), were purchased from Nanjing Jiancheng Bioengineering Institute (Nanjing, China). Primary antibodies against phosphorylated (p)-inhibitor of NF-κB-α (IκBα), IκBα, p-p65, p65, inducible nitric oxide synthase (iNOS), cyclooxygenase (COX)-2, nucleotide-binding domain-like receptor protein 3 (NLRP3), MMP2, MMP9, c-Fos, c-Jun, Lamin B1, GAPDH, heme oxygenase (HO)-1, and NAD(P)H:quinone oxidoreductase 1 (NQO1) were supplied by Cell Signaling Technology (Danvers, MA, USA), Abcam (Cambridge, UK), and Proteintech (Hubei, China), respectively. Cell Counting Kit (CCK)-8, ROS assay kit, total superoxide dismutase (SOD) assay kit, malondialdehyde (MDA) assay kit, and pharmacological inhibitors (pyrrolidinedithiocarbamate (PDTC) were procured from Beyotime Biotechnology (Shanghai, China). Incomplete Freund's adjuvant and bovine type II collagen were sourced from Chondrex, Inc. (Woodinville, WA, USA). Indomethacin (IND) was provided by Sigma-Aldrich (St. Louis, MO, USA). Pronase E (activity ≥ 7000 U·g^{-1}) and SR11302 were supplied by MedChemExpress (Monmouth Junction, NJ, USA).

2.2. Plant material and extraction

The ME herb was collected from Yunfu, Guangdong Province, China, and botanically authenticated by Prof. YU Hua. A voucher specimen (No. ME-001) has been deposited at the Institute of Chinese Medical Sciences, University of Macau, Macao SAR, China.

The air-dried ME herb was pulverized and subjected to reflux extraction with a 10-fold volume (*V/W*) of 75% ethanol, performed twice for 1 h per cycle. The combined filtrates were concentrated under reduced pressure and lyophilized to yield ME powder (extraction yield: 22.17%, *W/W*).

2.3. Ultra-performance liquid chromatography (UPLC) phytochemical profiling

Chromatographic analysis was performed using an ACQUITY UPLC CLASS system (Waters, USA) equipped with an ACQUITY UPLC BEH C18 column (150 mm × 2.1 mm, 1.7 μm). Separation was achieved *via* gradient elution with water (solvent A) and acetonitrile (solvent B) as follows: 0–3 min, 26% B; 3–5 min, 26%–37% B; 5–8 min, 37% B; 8–12 min, 37%–45% B. The flow rate was 0.35 mL·min^{-1}, and the injection volume was 2 μL. Detection was conducted at 324 nm, with the column temperature maintained at 45 °C. Between each run, the column was washed with 100% B for 2 min and re-equilibrated for 3 min under initial mobile phase conditions.

2.4. Animal experimentation

Male Wistar rats (7–8 weeks old) were housed under standard laboratory conditions with unrestricted access to food and water, a controlled temperature of 20–22 °C, 50% relative humidity, and a 12-h light/dark cycle. The CIA model was established by subcutaneous immunization with bovine type II collagen emulsified in incomplete Freund's adjuvant. An initial injection of 0.2 mL was administered at the base of the tail, followed by a 0.1 mL booster dose into the hind paws. Arthritis severity was assessed using a macroscopic scoring system, with scores ranging from 0 to 4 assigned to each paw based on the following criteria: 0, no arthritis; 1, swelling and/or redness in 1–2 interphalangeal (IP) joints; 2, involvement of 3–4 IP joints or one larger joint; 3, redness or swelling in more than 4 joints; and 4, severe arthritis affecting the entire paw. This yielded a total possible score of 0–16 per rat [18]. After modeling (total arthritis index > 4), rats were randomly assigned to six groups (n = 6 per group): Ctrl, CIA, CIA + ME-L (150 mg·kg^{-1}), CIA + ME-M (300 mg·kg^{-1}), CIA + ME-H (600 mg·kg^{-1}), and CIA + IND (2.5 mg·kg^{-1}, positive control). Treatments were administered daily *via* oral gavage for five weeks. Body weight and arthritis indices were monitored weekly, as previously described [19]. Terminal samples, including blood, joint muscles, spleen, liver, and kidneys, were collected for subsequent analyses.

2.5. Radiological and histopathological detection

On experimental day 57, bone structural integrity in the hind

paws was evaluated by micro-computed tomography (micro-CT) imaging. Following imaging, hind paw specimens were dissected to isolate muscle and bone compartments. Muscle tissue lysates were subjected to Western blotting analysis to quantify protein levels of MMP2, MMP9, NLRP3, c-Fos, c-Jun, p-p65, and p65. Bone samples were fixed in 10% neutral phosphate-buffered formalin and decalcified over 2–3 weeks using an acid solution. The decalcified samples were then processed for histopathological examination of joint damage using immunohistochemistry and hematoxylin and eosin (H&E) staining. Cartilage degradation was further assessed by Safranin O–fast green staining to quantify proteoglycan content, following standard methodologies [13].

2.6. Serum biomarker analysis

Serum concentrations of IgA, IgG, IL-6, IL-17/17A, MCP-1, TNF-α, and IL-10 were determined using ELISA kits according to the manufacturers' protocols.

Serum levels of AST, ALT, AKP, γ-GT, CRE, and BUN were quantified using commercial assay kits in accordance with standardized procedures.

2.7. Network pharmacology-based bioinformatic workflow

Chemical constituents of ME were retrieved from the CMAUP database (https://www.bidd.group/CMAUP/) and filtered based on Lipinski's rule of five: MW < 500, HBD ≤ 5, HBA ≤ 10, 0 < log*P* < 3, 1 < log*D* < 3, and rotatable bonds ≤ 10 [20]. SMILES notations of the filtered compounds were subjected to oral bioavailability evaluation *via* SwissADME (http://www.swissadme.ch/), focusing on compounds exhibiting high gastrointestinal (GI) absorption and meeting at least two drug-likeness criteria [21]. Putative targets of selected compounds were predicted using the SwissTargetPrediction (http://www.swisstargetprediction.ch/) and PubChem (https://pubchem.ncbi.nlm.nih.gov/) databases [22]. RA-associated genes were compiled from DisGeNET (https://www.disgenet.com/), GeneCards (https://www.genecards.org/), and OMIM (https://www.omim.org/), then intersected with ME-associated targets using the Venny tool (https://bioinfogp.cnb.csic.es/tools/venny/) to identify shared therapeutic targets.

The common targets were imported into the STRING database (https://cn.string-db.org/) to construct a protein–protein interaction (PPI) network (*Homo sapiens*; interaction score > 0.4). Network topology analysis was performed using Cytoscape 3.10.2 (https://cytoscape.org/) with core nodes identified by the CentiScape plugin. A multi-scale Herb–Compound–Target–Disease–Pathway network was visualized to prioritize compounds with the highest bioactivity scores.

Functional enrichment analysis was conducted *via* Metascape (https://metascape.org) with the following parameters: *Homo sapiens*, $P < 0.01$, and enrichment factor > 1.5. Kyoto Encyclopedia of Genes and Genomes (KEGG) pathways and Gene Ontology (GO) terms, including biological processes (BP), molecular functions (MF), and cellular components (CC), were visualized using the Bioinformatics platform (https://www.bioinformatics.com.cn).

2.8. Molecular docking validation of compound-target interactions

Molecular docking was performed to validate interactions between bioactive compounds and NF-κB p65 (gene name: *RELA*; UniProt ID: Q04206). The three-dimensional structure of p65 was retrieved from the PDB database (https://www.rcsb.org/; PDB ID: 2O61) and preprocessed using PyMOL 2.7.0. Compound structures, obtained from PubChem in SDF format, were converted to mol2 format using OpenBabel 3.1.1 with energy minimization. Following structural preparation, both protein and ligands were parameterized in AutoDockTools 1.5.7 for rigid docking simulations using AutoDock Vina 1.1.2. Binding conformations were visualized and analyzed in PyMOL 2.7.0 to characterize interaction modes and hydrogen bonding networks.

2.9. Cell culture

The human synovial sarcoma SW982 cell line, obtained from Procell Life Science & Technology Co., Ltd. (Hubei, China), was cultured in Dulbecco's modified Eagle's medium (DMEM) supplemented with 100 U·mL^{-1} penicillin/streptomycin (P/S) and 10% heat-inactivated fetal bovine serum (FBS). Cells were maintained at 37 °C in a humidified incubator with 5% CO_2/95% air and subcultured at 80%–90% confluence using 0.25% Trypsin-EDTA.

2.10. CCK-8 cytotoxicity assay and cytokine release analysis

SW982 cells were seeded into 96-well plates at a density of 1×10^4 cells per well and allowed to adhere for 24 h. Cells were then exposed to ME extract at varying concentrations with or without IL-1β (25 ng·mL^{-1}) for 24 or 48 h. Post-treatment, culture supernatants were collected for quantification of TNF-α, IL-6, IL-8, and IL-1β using specific ELISA kits. Cell viability was assessed by adding CCK-8 reagent-containing medium and measuring absorbance at 450 nm.

2.11. Scratch wound healing assay

SW982 cells were seeded into 96-well plates at a density of 2×10^4 cells per well to form a confluent monolayer. Uniform wounds were generated using a WoundMaker™ (Sartorius, Germany). After removing non-adherent cells with phosphate-buffered saline (PBS), initial wounds were recorded using an IncuCyte® S3 Live-Cell Analysis System (Sartorius, Germany). Cells were subsequently treated with ME extract (30, 60, and 120 μg·mL^{-1}) with or without IL-1β (25 ng·mL^{-1}). Following a 24-h incubation, wounds were re-imaged, and wound closure was quantified using Photoshop software by calculating the percentage reduction in wound area.

2.12. Transwell migration assay

Cell migration capacity was evaluated using 8-μm pore Transwell chambers (SPL Life Sciences, Korea). SW982 cells pretreated with ME extract (30, 60, or 120 μg·mL^{-1}) in the presence or absence of IL-1β (25 ng·mL^{-1}) in serum-free DMEM were loaded into upper chambers (5×10^4 cells/200 μL), while lower chambers contained DMEM with 10% FBS (600 μL). After 24 h of incubation, non-migrated cells were mechanically removed. Membranes were fixed with 4% paraformaldehyde, stained with crystal violet, and the migrated cells were counted across three independent experiments.

2.13. Intracellular ROS measurement

SW982 cells were plated into 12-well plates (2×10^5 cells/well). Following 24 h of drug treatment, cells from each group were collected and incubated with 10 μmol·L^{-1} 2′,7′-dichlorodihydrofluorescein diacetate (DCFH-DA) for 30 min in the dark. After washing with PBS, intracellular ROS levels were quantified by flow cytometry.

2.14. Oxidative stress biomarker analysis

Concentrations of oxidative stress biomarkers (SOD and MDA) in cell lysates or rat joint muscle tissues were measured according to the manufacturers' protocols.

2.15. Quantitative real-time polymerase chain reaction (qRT-PCR) analysis

Total ribonucleic acid (RNA) was extracted from SW982 cells and reverse-transcribed into complementary deoxyribonucleic acid (cDNA). The synthesized cDNA was used to assess messenger ribonucleic acid (mRNA) levels of inflammatory cytokines (TNF-α, IL-6, IL-8, and IL-1β) in each sample. GAPDH mRNA served as the internal control, and relative mRNA expression was calculated using the $2^{-\Delta\Delta Ct}$ method. Gene-specific primers, designed and synthesized by Guangzhou Ige Biotechnology, Ltd. (Guangdong, China), are detailed in Table 1.

Table 1 Primer sequences employed in our research.

Primer name	Sequence (5′-3′)
Human *TNF-α*	Forward: CCTCTCTCTAATCAGCCCTCTG
	Reverse: GAGGACCTGGGAGTAGATGAG
Human *IL-6*	Forward: ACTCACCTCTTCAGAACGAATTG
	Reverse: CCATCTTTGGAAGGTTCAGGTTG
Human *IL-8*	Forward: TTTTGCCAAGGAGTGCTAAAGA
	Reverse: AACCCTCTGCACCCAGTTTTC
Human *IL-1β*	Forward: ATGATGGCTTATTACAGTGGCAA
	Reverse: GTCGGAGATTCGTAGCTGGA
Human *GAPDH*	Forward: AGATCCCTCCAAAATCAAGTGG
	Reverse: GGCAGAGATGATGACCCTTTT

2.16. Total protein extraction and Western blotting analysis

SW982 cells were collected and lysed in an appropriate lysis buffer. Protein extracts (about 30 μg per sample) were separated by electrophoresis on a 10% sodium dodecyl sulfate-polyacrylamide gel electrophoresis (SDS-PAGE) gel and transferred onto polyvinylidene fluoride (PVDF) membranes. After blocking non-specific binding sites, membranes were incubated overnight at 4 °C with specific primary antibodies, followed by corresponding secondary antibodies for 1 h at room temperature (RT). Protein bands were visualized and quantified using a Gel Imaging System (Bio-Rad, USA).

2.17. Immunofluorescence staining

To assess protein expression and nuclear translocation of NF-κB p65 in SW982 cells induced by IL-1β, immunofluorescence staining was performed according to a previously established protocol [23]. Stained samples were examined using confocal laser microscopy (Leica, USA) for visualization and quantification.

2.18. Cellular thermal shift assay (CETSA) analysis

Lysates from SW982 cells (about 3 mg·mL^{-1}) were prepared and incubated overnight at 4 °C with ME extract (120 μg·mL^{-1}) or vehicle control (dimethyl sulfoxide, DMSO) under constant shaking. Subsequently, 450 μL of the protein–extract mixture was aliquoted into 50 μL portions and heat-treated using a thermal cycler (Eppendorf, USA). Samples were exposed to incrementally increasing temperatures from 45 °C to 85 °C in 5 °C steps, with each temperature maintained for 5 min. After centrifugation, 40 μL of the protein supernatant from each aliquot was mixed with 10 μL of 5 × SDS-PAGE sample loading buffer. Protein thermal stability was assessed by Western blotting to generate thermal denaturation profiles.

2.19. Drug affinity responsive target stability (DARTS) assay

The DARTS assay was performed with modifications to a published protocol [24]. SW982 cell lysates (2.5–4 mg·mL^{-1}) were incubated with ME extract (120 μg·mL^{-1}) or vehicle control (DMSO) for 2 h at RT. Limited proteolysis was initiated by adding Pronase E solution (20 μg·mL^{-1} final concentration) and allowed to proceed for 30 min at RT. The pronase-induced digestion reaction was terminated by adding 5 × SDS-PAGE loading buffer, followed by heat denaturation at 100 °C for 5 min. Protease susceptibility of target proteins was evaluated by Western blotting analysis.

2.20. Statistical analysis

Data from at least three independent experiments are presented as mean ± SEM. Intergroup comparisons were performed using GraphPad Prism 8.0 software, employing one-way ANOVA to evaluate differences among experimental groups. A P value of less than 0.05 was considered statistically significant.

3. Results

3.1. Phytochemical profiling of ME extract

The representative UPLC chromatograms of the mixed standards and ME extract are shown in Fig. S1. The contents of meranzin hydrate, hainanmurpanin, murrayone, and 3',4',5,5',6,7-hexamethoxyflavone were quantified as 2.86% ± 0.01%, 1.88% ± 0.01%, 0.07% ± 0.00%, and 0.01% ± 0.00%, respectively.

3.2. Therapeutic efficacy of ME extract in CIA rats

The experimental timeline is schematically represented in Fig. 1A. Following two consecutive injections of bovine type II collagen over a three-week period, arthritis indices in model rats exceeded 4, whereas those in control rats remained at 0, confirming successful establishment of the CIA rat model. Subsequently, CIA rats were administered ME extract or IND for five weeks to evaluate their therapeutic effects against RA. Throughout the treatment period, no adverse effects on animal growth were observed (Fig. 1B). Serum levels of AST, ALT, ALP, γ-GT, CRE, and BUN remained comparable across groups, although IND administration significantly reduced AST levels in CIA rats (Figs. 1C–1D). Furthermore, histopathological examination of spleen, liver, and kidney sections *via* H&E staining revealed preserved tissue architecture without significant pathological abnormalities in all groups (Fig. 1E). These findings indicate that neither ME nor IND at the administered dosages induced significant damage to major rat organs, highlighting their acceptable toxicological safety profiles. Additionally, data in Figs. 1F–1G demonstrate a progressive decline in both arthritis indices and hind paw swelling following oral administration of ME extract or IND.

3.3. Histopathological evaluation of ME extract on joint damage in CIA rats

Micro-CT imaging of hind paw joints indicated that treatment with ME extract or IND significantly mitigated bone erosion and joint destruction in CIA rats (Fig. 2A). Detailed histological examination (H&E and Safranin O–fast green staining) of toe and ankle joints revealed that control rats maintained normal joint architecture with distinct articular spaces. In contrast, CIA rats exhibited severe synovial hyperplasia, narrowed articular spaces, cartilage degradation, and extensive bone erosion. Notably, ME extract or IND treatment markedly attenuated synovial cell hy-

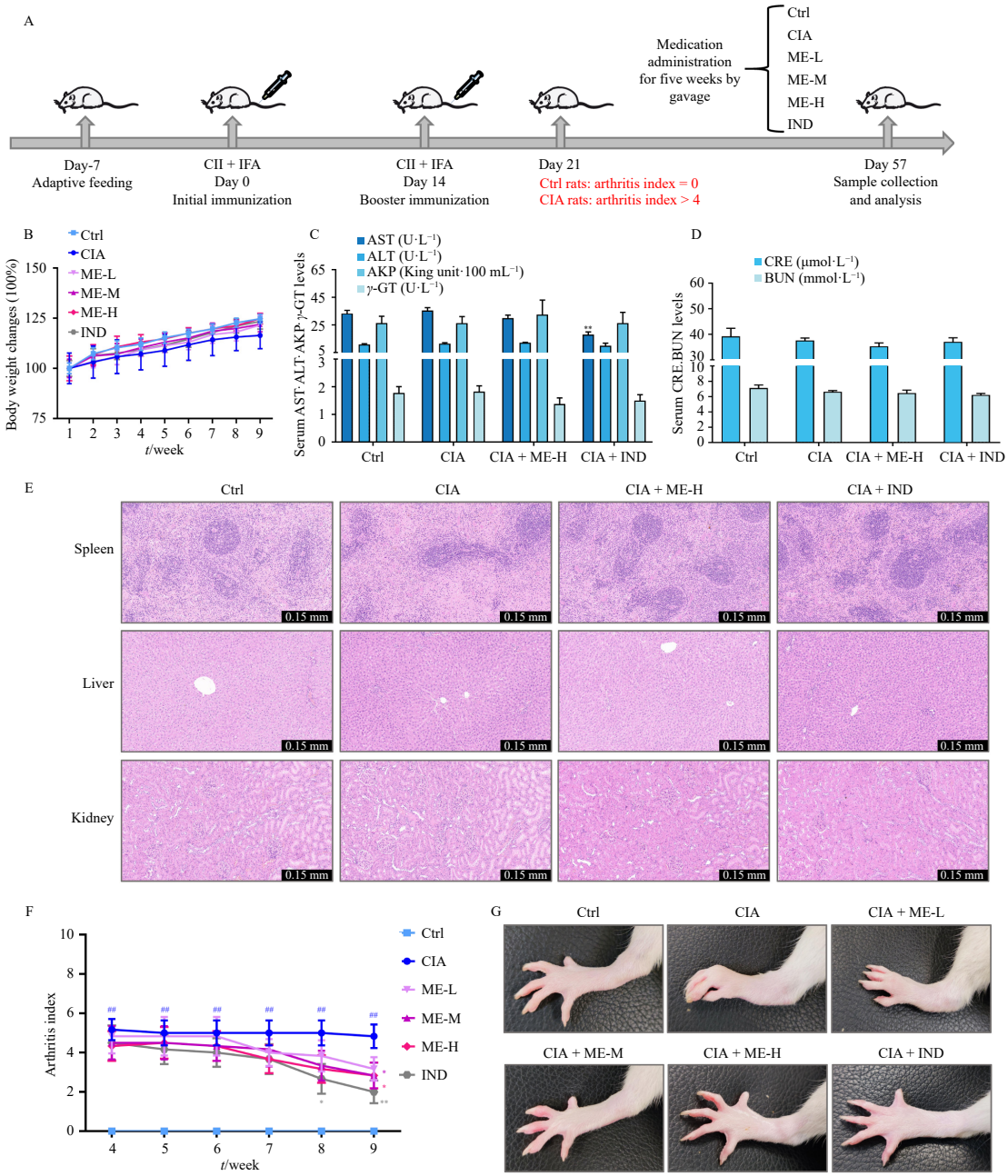

Fig. 1 Therapeutic efficacy of ME extract in CIA rats. (A) Experimental protocol for *in vivo* studies. (B) Growth curve of CIA rats (n = 6). (C–D) Detection of serum biochemical parameters (AST, ALT, AKP, γ-GT, CRE, and BUN) in CIA rats (n = 6). (E) Histopathological examination of spleen, liver, and kidney *via* H&E staining. (F–G) Assessment of the arthritis index and hind paw swelling in CIA rats (n = 6). The results are presented as the mean ± SEM. $^{\#}P < 0.05$ and $^{\#\#}P < 0.01$ *vs* Ctrl; $^{*}P < 0.05$ and $^{**}P < 0.01$ *vs* CIA group.

perproliferation, reduced inflammatory infiltration, and alleviated cartilage and bone damage, suggesting the therapeutic potential of ME in ameliorating RA-related joint pathology (Figs. 2B–2D).

3.4. Modulation of ME extract on inflammatory response in CIA rats

As shown in Figs. 3A–3G, administration of ME extract or IND significantly reduced serum levels of autoantibodies (IgA and IgG) and pro-inflammatory cytokines (IL-6, IL-17/17A, MCP-1, and TNF-α) in CIA rats, while increasing the anti-inflammatory cytokine IL-10. Additionally, IL-2, IL-1β, MCP-1, and TNF-α levels in joint-associated muscles were measured using specific ELISA kits. Both ME extract and IND treatment significantly normalized the aberrant expression of these pro-inflammatory cytokines in the joint muscles of CIA rats to varying degrees (Figs. 3H–3K).

3.5. Suppression of ME extract on IL-1β-triggered proliferation/migration in SW982 cells

To investigate the mechanisms underlying ME's protective effects observed in CIA rats, *in vitro* experiments were performed. CCK-8 assay results revealed that IL-1β was more potent than TNF-α in stimulating synovial cell proliferation at equivalent concentrations and exposure durations (Fig. 4A). After a 24-h treatment, ME extract at concentrations of 125 μg·mL^{-1} and above began to affect SW982 cell viability (Fig. 4B). Based on existing literature and preliminary studies, IL-1β (25 ng·mL^{-1}, 24 h) was selected to induce the inflammatory model, with low (30 μg·mL^{-1}), medium (60 μg·mL^{-1}), and high (120 μg·mL^{-1}) doses of ME extract applied as protective interventions (ensuring cell viability > 85%). As demonstrated in Fig. 4C, ME extract effectively suppressed IL-1β-triggered abnormal synovial cell proliferation in a dose-dependent manner. Furthermore, scratch wound heal-

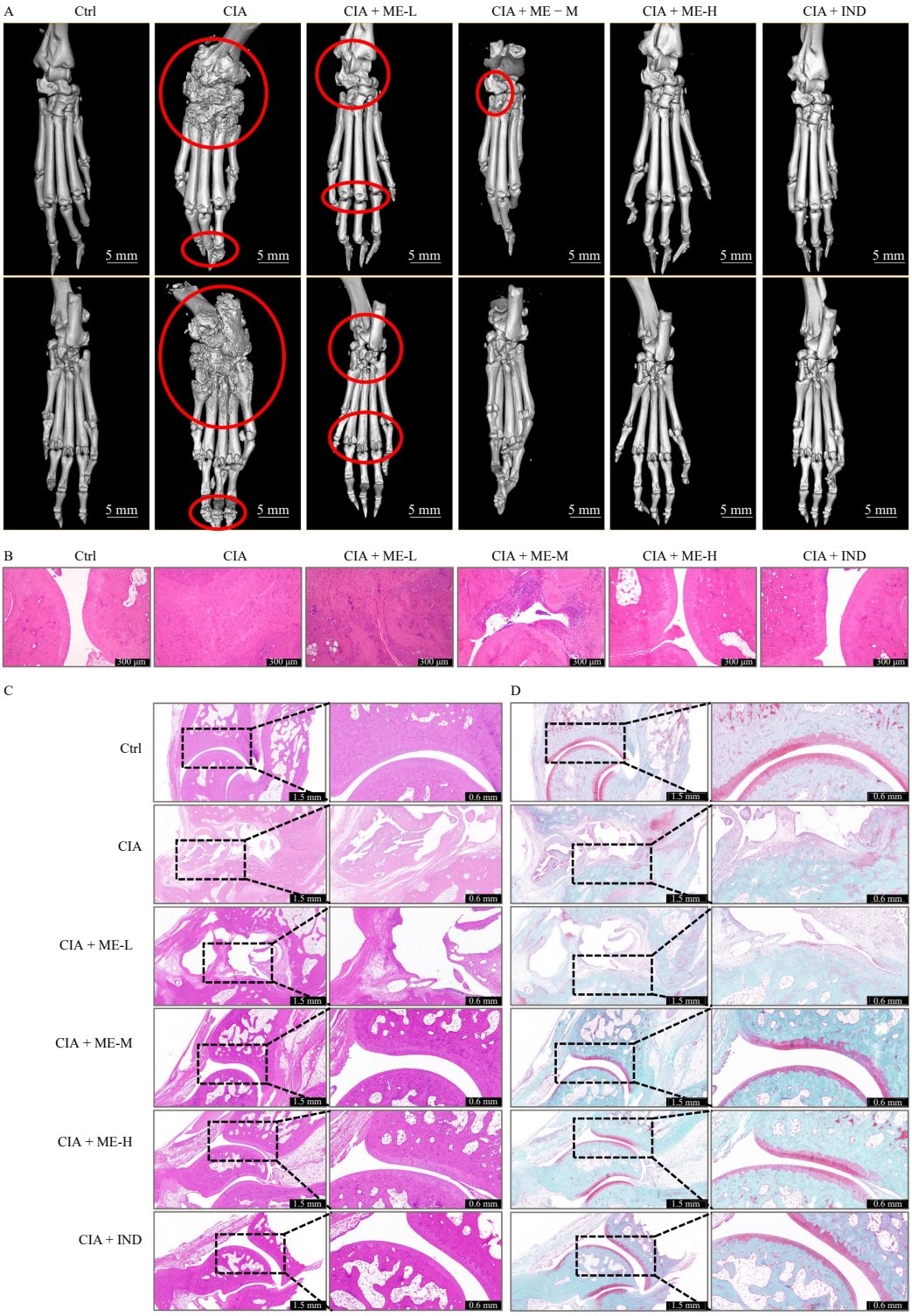

Fig. 2 Histopathological evaluation of ME extract on joint damage in CIA rats. (A) Micro-CT imaging of hind paws. (B–C) Histological examination of the toe and ankle joint damage *via* H&E staining. (D) Determination of cartilage degeneration in ankle joints through Safranin O staining.

ing and transwell assays confirmed that ME extract markedly inhibited IL-1β-induced SW982 cell migration in a concentration-dependent fashion (Figs. 4D–4G).

3.6. Downregulation of ME extract on MMP2/MMP9 expression in IL-1β-triggered SW982 cells/CIA rats

Elevated MMP2 and MMP9 levels are closely associated with the migration and invasion of RA-FLSs, establishing these proteases as critical therapeutic targets in RA treatment [25]. As shown in Figs. 5A–5C, ME extract markedly inhibited IL-1β-induced overexpression of MMP2 and MMP9 in SW982 cells. Additionally, Western blotting and immunohistochemical analyses confirmed that both ME extract and IND attenuated the upregulation of MMP2 and MMP9 expression to varying degrees in joint muscles and ankle tissues of arthritic rats (Figs. 5D–5H).

3.7. Inhibition of ME extract on IL-1β-triggered inflammatory response in SW982 cells

ELISA results revealed that ME extract (30–120 μg·mL^{-1}) dose-dependently reduced the extracellular release of inflammat-

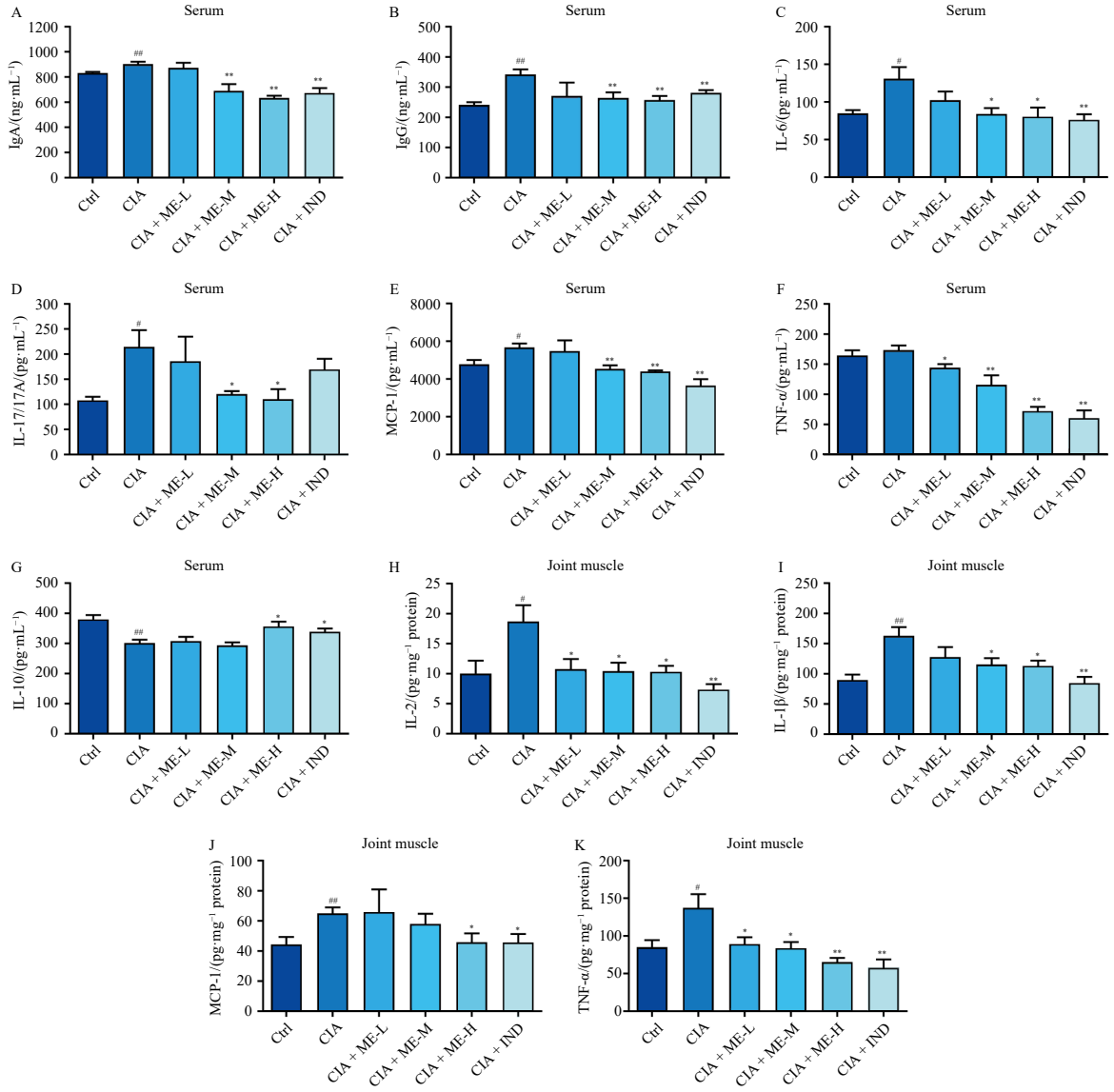

Fig. 3 Modulation of ME extract on inflammatory response in CIA rats. (A–G) Measurement of IgA, IgG, IL-6, IL-17/17A, MCP-1, TNF-α, and IL-10 in the serum of CIA rats using ELISA (n = 6). (H–K) Detection of IL-2, IL-1β, MCP-1, and TNF-α in the joint-associated muscles of CIA rats using ELISA (n = 6). The results are presented as the mean ± SEM. $^{\#}P < 0.05$ and $^{\#\#}P < 0.01$ *vs* Ctrl; $^{*}P < 0.05$ and $^{**}P < 0.01$ *vs* CIA group.

ory cytokines (TNF-α, IL-6, IL-8, and IL-1β) (Fig. 6A). Consistently, qRT-PCR analysis showed a comparable dose-dependent reduction in intracellular mRNA levels of these cytokines, suggesting that ME exerts coordinated anti-inflammatory effects at both extracellular and intracellular levels (Fig. 6B). Given the established roles of NLRP3, iNOS, and COX-2 in RA pathogenesis [13, 19], we evaluated their expression under IL-1β stimulation. As illustrated in Figs. 6C–6F, IL-1β induced a marked increase in these inflammation-associated proteins, which was dose-dependently suppressed by ME extract.

3.8. Amelioration of ME extract on oxidative stress in IL-1β-triggered SW982 cells/CIA rats

Oxidative stress, driven by interactions between the immune system and endogenous or exogenous antigens in autoimmune disorders, is a key pathogenic factor in RA progression [26]. IL-1β stimulation significantly increased ROS and MDA (a biomarker of lipid peroxidation) levels in SW982 cells, whereas ME treatment dose-dependently reduced these oxidative markers (Figs. 7A–7B). Furthermore, ME markedly upregulated the expression of antioxidant proteins HO-1 and NQO1 compared to the IL-1β group (Figs. 7C–7E). Consistently, ME enhanced SOD (a key antioxidant enzyme) activity while decreasing MDA concentration in joint tissues of CIA rats (Figs. 7F–7G). Collectively, these findings indicate that ME exerts beneficial effects in alleviating RA-associated oxidative stress.

3.9. Bioinformatic insights from network pharmacology and molecular docking investigations

Integrated network pharmacology and molecular docking analyses identified key bioactive components and therapeutic targets of ME in RA treatment. Twenty-five ME-derived compounds meeting GI absorption criteria were curated from the CMAUP database (Table 2). Target prediction using the SwissTargetPrediction and PubChem databases yielded 614 ME-associated targets, while 1643 RA-related targets were retrieved from DisGeNET, GeneCards, and OMIM databases. Venn diagram analysis revealed 221 overlapping genes between ME and RA (Fig. 8A). GO enrichment highlighted the top 10 terms for BP, MF, and CC (Fig. 8B). KEGG pathway analysis (top 20 pathways, $P < 0.01$) identified the NF-κB signaling pathway as the central mechanism (Fig. 8C). Protein-protein interaction (PPI) network analysis *via* the STRING 12.0 database prioritized *RELA* as a pivotal target. A multi-layer network (255 nodes: 40 core target nodes, 181 inter-

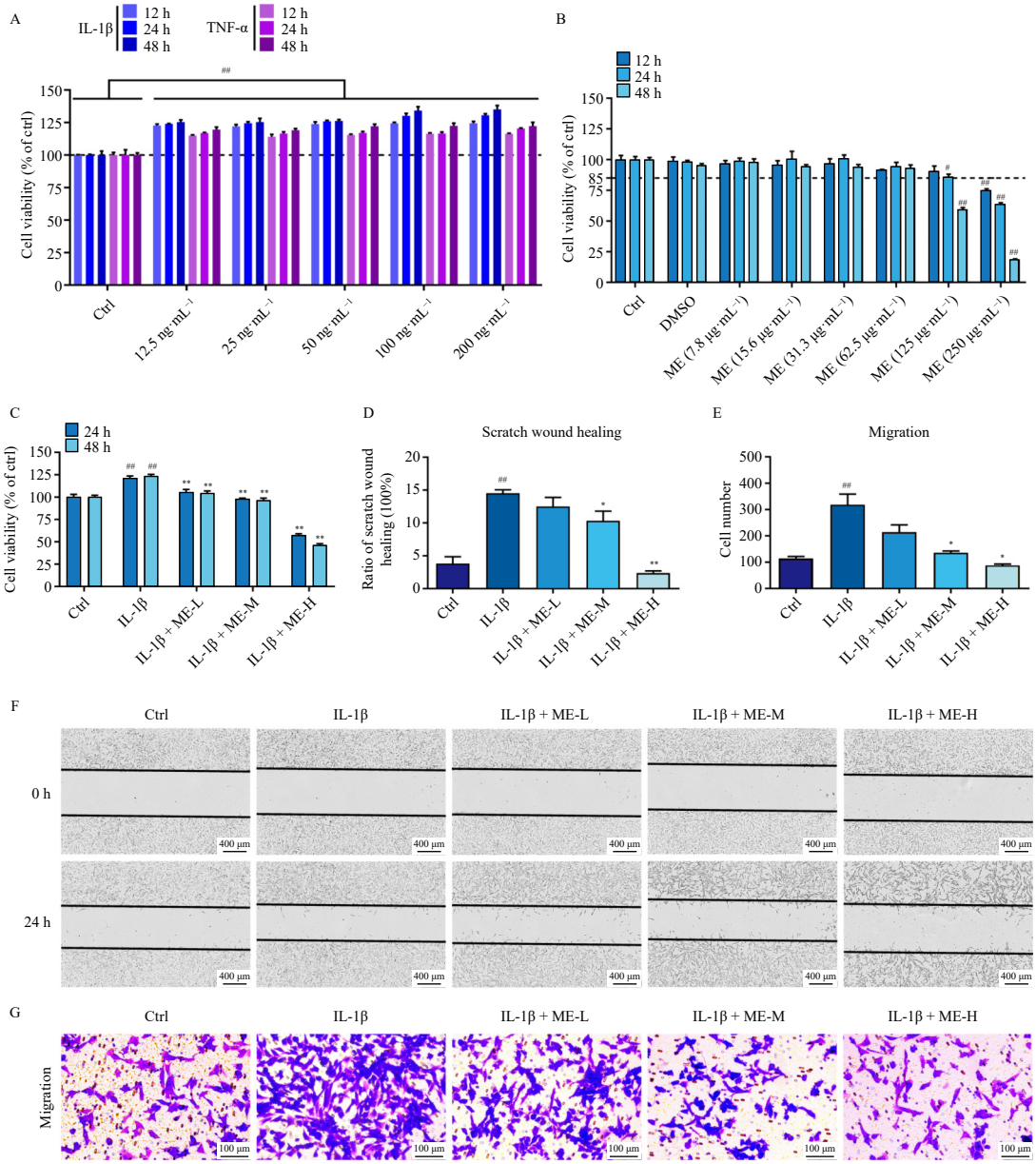

Fig. 4 Suppression of ME extract on IL-1β-triggered proliferation/migration in SW982 cells. (A) The proliferative effects of IL-1β/TNF-α on SW982 cells (n = 3). (B) The cytotoxicity of ME extract in SW982 cells (n = 3). (C) Suppression of IL-1β-triggered proliferation by ME extract (n = 4). (D–G) Inhibition of IL-1β-triggered migration by ME extract (n = 3). The results are presented as the mean ± SEM. $^{\#}P < 0.05$ and $^{\#\#}P < 0.01$ *vs* Ctrl; $^{*}P < 0.05$ and $^{**}P < 0.01$ *vs* IL-1β group.

secting target nodes, 25 active compound nodes, 7 pathway nodes, 1 herb node, and 1 disease node; 1413 edges) mapped interactions among compounds, targets, and pathways, with degree centrality analysis identifying genistein, [(1R,2S)-1-hydroxy-1-(7-methoxy-2-oxochromen-8-yl)-3-methylbut-3-en-2-yl] 3-methylbutanoate, murrayone, and others as core bioactive compounds in ME (Table 3).

Molecular docking studies (binding energy ≤ −5.0 kcal·mol^{-1} as cutoff) demonstrated strong binding affinities between all 11 top-ranked compounds and NF-κB p65 (Figs. 8D–8N). CETSA analysis revealed that ME binding stabilized p65 against thermal denaturation (Tm (ME-H) = 78.53 °C *vs* Tm (DMSO) = 72.50 °C; Figs. 9A–9B). DARTS analysis showed that ME protected p65 from pronase-mediated proteolysis (Figs. 9C–9D). Collectively, these findings confirm that ME directly targets NF-κB p65, thereby inhibiting NF-κB pathway activation in RA.

3.10. Regulation of ME extract on NF-κB/activator protein-1 (AP-1) signaling pathways in IL-1β-triggered SW982 cells/CIA rats

Based on the results shown in Figs. 8–9, the NF-κB signaling pathway appears to play a pivotal role in the ME-mediated anti-RA effects. As presented in Figs. 10A–10C, IL-1β stimulation induced IκBα phosphorylation and degradation and elevated p-p65 levels, which were significantly suppressed by ME treatment. Figs. 10D–10E provides evidence that ME notably reduced nuclear p65 accumulation and blocked its nuclear translocation in IL-1β-stimulated SW982 cells, as demonstrated by Western blotting and immunofluorescence analyses. Furthermore, ME effectively downregulated IL-1β-induced overexpression of c-Fos and c-Jun in SW982 cells (Figs. 10F–10H). Consistent with *in vitro* observations, ME administration suppressed NLRP3 expression and inhibited NF-κB/AP-1 pathway activation in CIA rats (Figs. 10I–10J).

3.11. NF-κB/AP-1 pathway modulation underpinned ME's anti-proliferative, anti-inflammatory, and anti-oxidative effects

The specific NF-κB inhibitor (PDTC, 10 μmol·L^{-1}) and AP-1 inhibitor (SR11302, 2.5 μmol·L^{-1}) were employed to further validate the mechanistic roles of NF-κB and AP-1. As depicted in

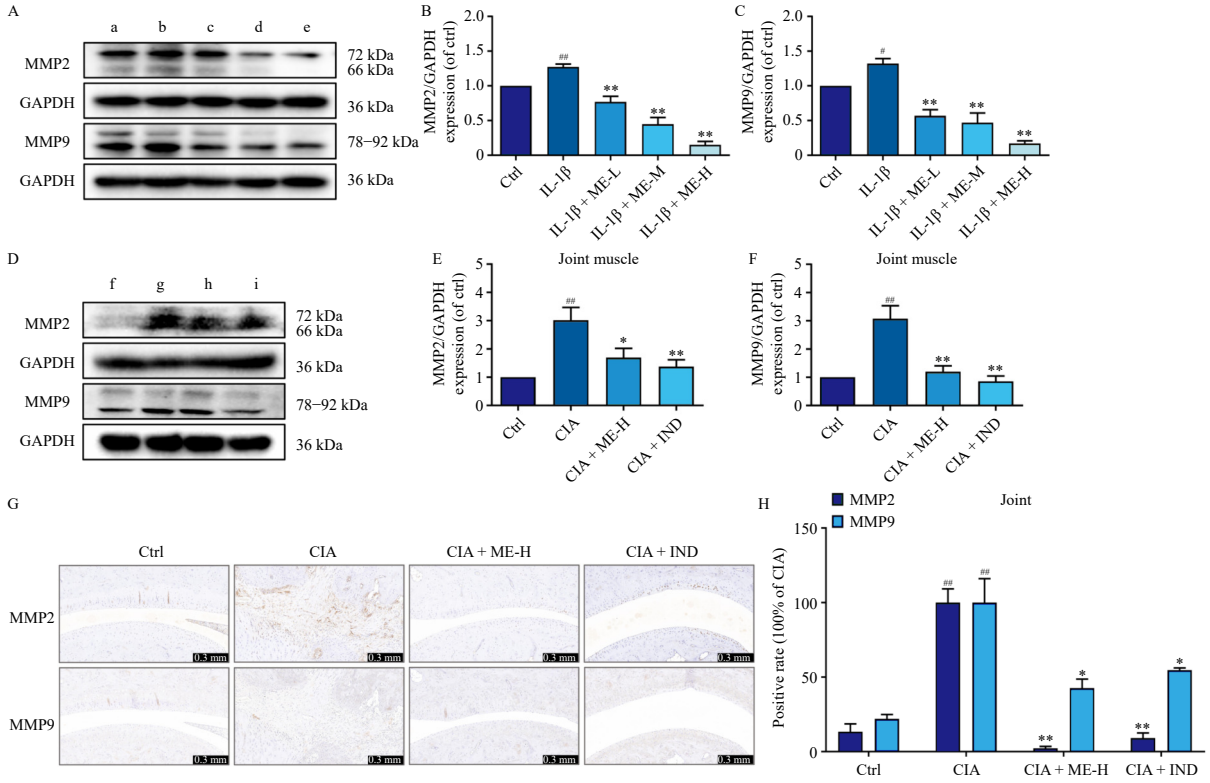

Fig. 5 Downregulation of ME extract on MMP2/MMP9 expression in IL-1β-triggered SW982 cells/CIA rats. (A–F) Evaluation of MMP2 and MMP9 levels in IL-1β-triggered SW982 cells (n = 3) and joint muscles of CIA rats (n = 6) *via* Western blotting. (G–H) Detection of MMP2 and MMP9 expressions in the ankle joints of CIA rats through immunohistochemistry (n = 3). The results are presented as the mean ± SEM. $^{\#}P < 0.05$ and $^{\#\#}P < 0.01$ *vs* Ctrl; $^{*}P < 0.05$ and $^{**}P < 0.01$ *vs* IL-1β or CIA group. (a: Ctrl; b: IL-1β; c: IL-1β + ME-L; d: IL-1β + ME-M; e: IL-1β + ME-H; f: Ctrl; g: CIA; h: CIA + ME-H; i: CIA + IND).

Figs. 11A–11E, ME extract effectively mitigated IL-1β-stimulated synovial cell proliferation and migration, paralleling the effects of PDTC or SR11302. Similarly, ME extract markedly attenuated IL-1β-driven inflammatory cytokine release and ROS overproduction, matching the efficacy of these inhibitors (Figs. 11F–11G). These findings indicate that the protective effects of ME extract were analogous to the anti-proliferative, anti-inflammatory, and anti-oxidative actions exerted by PDTC or SR11302 in IL-1β-stimulated synovial cells.

Notably, the combination of ME with PDTC exhibited no additive effect on nuclear p65 suppression (Figs. 11H–11I). Similarly, ME combined with SR11302 inhibited c-Fos/c-Jun expression without significant intergroup differences (Fig. 11J). Collectively, these findings demonstrate that ME's therapeutic benefits in RA are mediated through dual inhibition of the NF-κB/AP-1 signaling pathways.

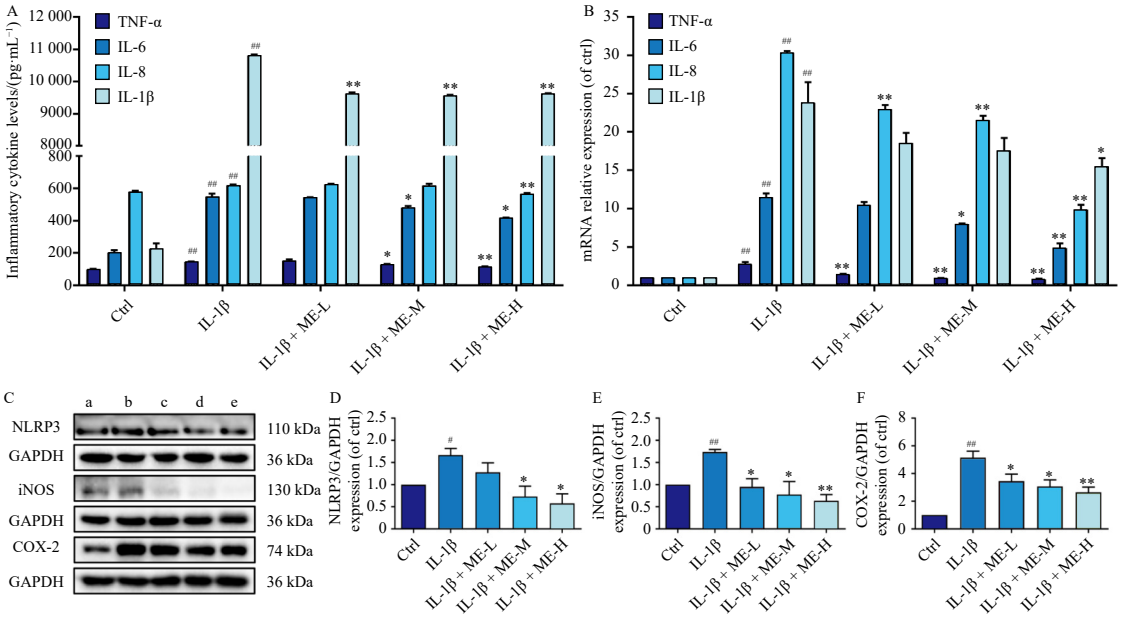

Fig. 6 Inhibition of ME extract on IL-1β-triggered inflammatory response in SW982 cells. (A) Detection of TNF-α, IL-6, IL-8, and IL-1β in the culture supernatants of IL-1β-triggered SW982 cells by ELISA (n = 3). (B) Assessment of mRNA levels of TNF-α, IL-6, IL-8, and IL-1β in IL-1β-triggered SW982 cells by qRT-PCR (n = 3). (C–F) Determination of protein expressions of inflammation-related markers (NLRP3, iNOS, and COX-2) in IL-1β-triggered SW982 cells by Western blotting (n = 3). The results are presented as the mean ± SEM. $^{\#}P < 0.05$ and $^{\#\#}P < 0.01$ *vs* Ctrl; $^{*}P < 0.05$ and $^{**}P < 0.01$ *vs* IL-1β group. (a: Ctrl; b: IL-1β; c: IL-1β + ME-L; d: IL-1β + ME-M; e: IL-1β + ME-H).

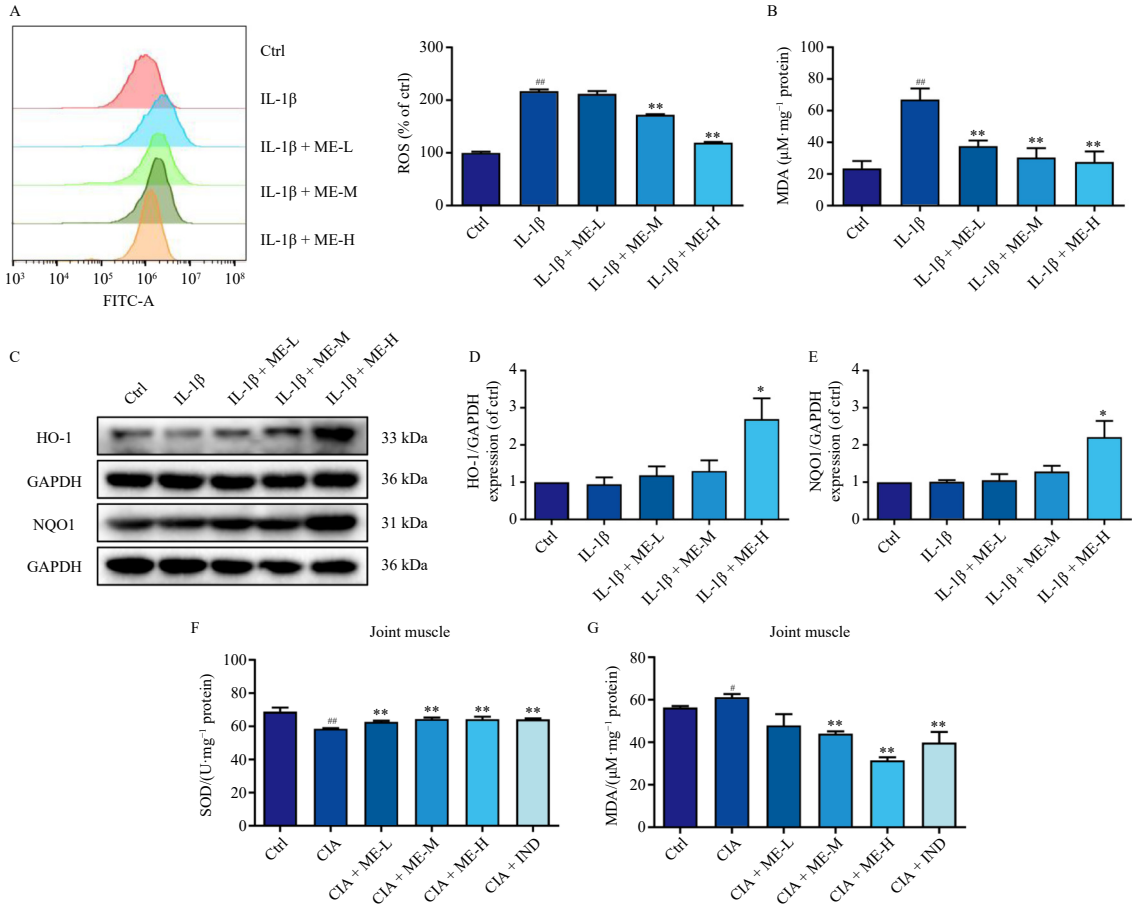

Fig. 7 Amelioration of ME extract on oxidative stress in IL-1β-triggered SW982 cells/CIA rats. (A–B) Measurement of ROS and MDA levels in IL-1β-triggered SW982 cells (n = 4). (C–E) Evaluation of HO-1 and NQO1 expressions in IL-1β-triggered SW982 cells by Western blotting (n = 6). (F–G) Detection of SOD and MDA concentrations in the joint muscles of CIA rats (n = 6). The results are presented as the mean ± SEM. $^{\#}P < 0.05$ and $^{\#\#}P < 0.01$ *vs* Ctrl; $^{*}P < 0.05$ and $^{**}P < 0.01$ *vs* IL-1β or CIA group. (a: Ctrl; b: IL-1β; c: IL-1β + ME-L; d: IL-1β + ME-M; e: IL-1β + ME-H).

Table 2 25 bioactive compounds in *Murraya exotica* L. (ME)

No.	CMAUP ID	Compound Name	Molecular Formula	PubChem CID
1	NPC85233	Nobiletin	$C_{21}H_{22}O_8$	72344
2	NPC68889	Linalool, (-)-	$C_{10}H_{18}O$	443158
3	NPC61225	3-Octen-1-OL	$C_8H_{16}O$	5364475
4	NPC484109	n.a.	$C_{28}H_{30}O_6$	n.a.
5	NPC484108	n.a.	$C_{28}H_{30}O_6$	n.a.
6	NPC39426	Genistein	$C_{15}H_{10}O_5$	5280961
7	NPC307253	8-Hydroxycoumarin	$C_9H_6O_3$	122783
8	NPC294902	Caffeic Acid	$C_9H_8O_4$	689043
9	NPC284478	5-Isopropylbicyclo[3.1.0]hex-2-ene-2-carbaldehyde	$C_{10}H_{14}O$	530411
10	NPC271600	7-Methoxy-8-[(1E)-3-oxobut-1-EN-1-YL]chromen-2-one	$C_{14}H_{12}O_4$	71434712
11	NPC257124	Eugenol	$C_{10}H_{12}O_2$	3314
12	NPC2476	5-Demethylnobiletin	$C_{20}H_{20}O_8$	358832
13	NPC246358	2-Methoxy-4-vinylphenol	$C_9H_{10}O_2$	332
14	NPC242701	(3Z)-Oct-3-EN-1-OL	$C_8H_{16}O$	28937
15	NPC234560	Daidzein	$C_{15}H_{10}O_4$	5281708
16	NPC201547	3,5,6,7,8,3',4'-Heptamethphoxyflavone	$C_{22}H_{24}O_9$	150893
17	NPC183864	Murrayone	$C_{15}H_{14}O_4$	5319964
18	NPC182943	Phellandral	$C_{10}H_{16}O$	89488
19	NPC180871	Linalool, (+ /-)-	$C_{10}H_{18}O$	6549
20	NPC16721	p-Menth-1(7)-en-2-one	$C_{10}H_{16}O$	557612
21	NPC165320	cis-3-Octen-1-ol	$C_8H_{16}O$	5364519
22	NPC139546	Linalool, (+)-	$C_{10}H_{18}O$	67179
23	NPC129572	[(1R,2S)-1-hydroxy-1-(7-methoxy-2-oxochromen-8-yl)-3-methylbut-3-en-2-yl] 3-methylbutanoate	$C_{20}H_{24}O_6$	14779479
24	NPC116775	Kaempferol	$C_{15}H_{10}O_6$	5280863
25	NPC1075	cis-Caffeic acid	$C_9H_8O_4$	1549111

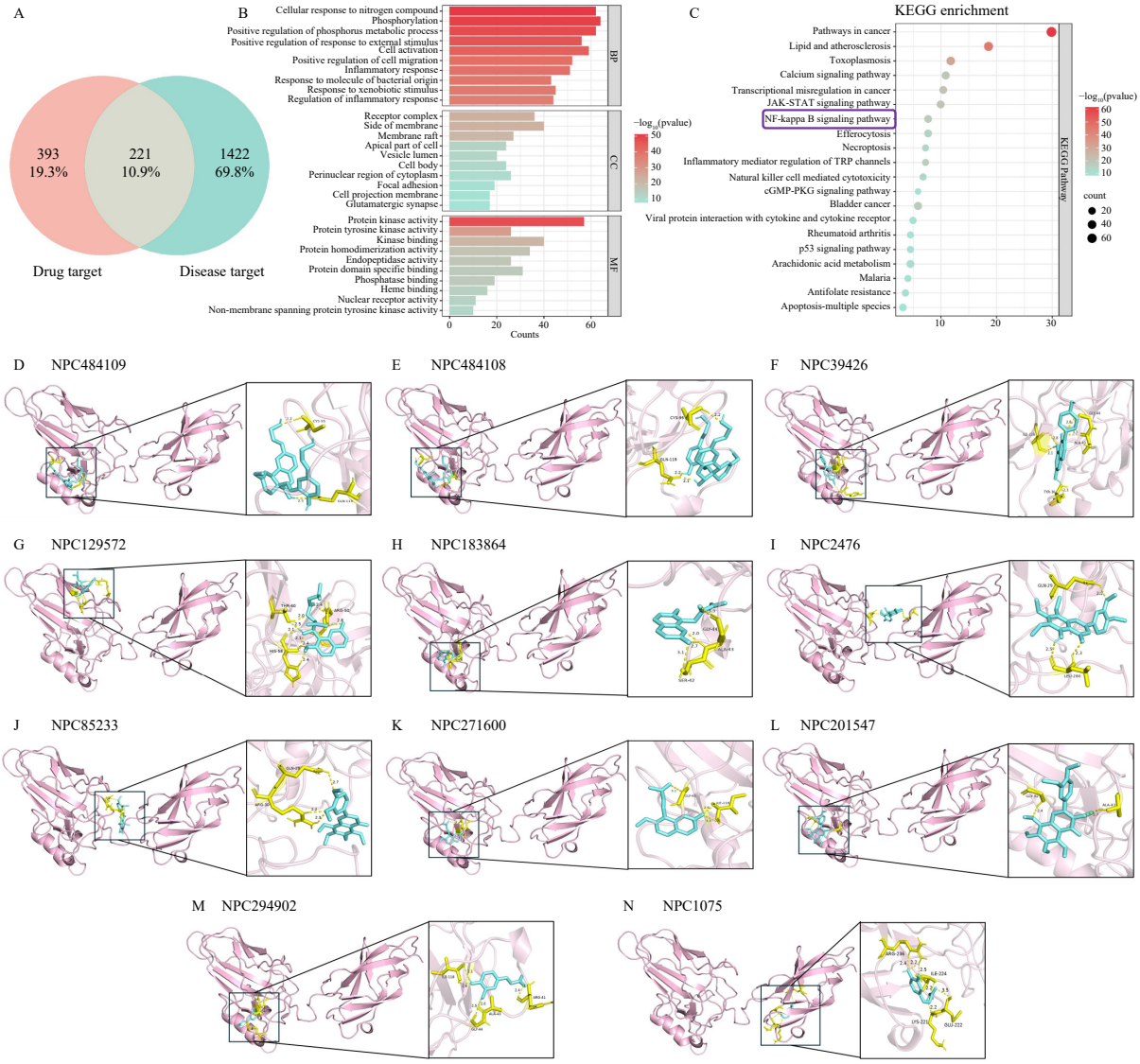

Fig. 8 Bioinformatic insights from network pharmacology and molecular docking investigations. (A) Venn diagram illustrating drug-disease targets. (B–C) GO and KEGG analyses of the identified drug-disease targets. (D–E) PPI network of the overlapping drug-disease targets. (F) An integrated Herb-Compound-Target-Disease-Pathway network. (G–Q) Molecular docking of 11 active compounds in ME with the target protein p65.

4. Discussion

The current study elucidates the multifaceted therapeutic potential of ME extract in RA, integrating chemical characterization, *in vivo*/*in vitro* efficacy validation, and mechanistic insights into its NF-κB/AP-1 pathway-mediated anti-proliferative, anti-inflammatory, and anti-oxidative properties. Below, we contextualize these findings within the broader landscape of RA therapeutics and propose actionable strategies for the clinical development of ME.

The safety profile of ME extract is particularly noteworthy. No significant hepatotoxicity or nephrotoxicity was observed in CIA rats, even after prolonged administration. AST, ALT, AKP, γ-GT, CRE, and BUN are key biochemical markers that reflect liver and kidney function, playing critical roles in the assessment of organ health [27]. Specifically, ME extract did not induce adverse effects on animal growth or organ function, as evidenced by unchanged serum biochemical parameters (AST, ALT, AKP, γ-GT, CRE, and BUN) and histopathological analyses (H&E staining of spleen, liver, and kidney tissues). This contrasts with conventional DMARDs such as methotrexate (MTX), which often require rigorous monitoring due to hepatic and hematologic side effects [28]. This favorable safety profile positions ME as a promising candidate for long-term RA management, particularly in patients with comorbidities requiring hepatorenal protection.

Immunoglobulins (IgA and IgG) are antibody-active proteins that serve as critical biomarkers for RA disease activity [29]. The anti-inflammatory effects of ME extract were corroborated by its ability to downregulate pro-inflammatory cytokines (IL-6, IL-17A, MCP-1, and TNF-α) and autoantibodies (IgA and IgG), while upregulating the anti-inflammatory cytokine IL-10 in the serum of CIA rats. Moreover, ME extract significantly ameliorated the elevated expression of pro-inflammatory cytokines (IL-2, IL-1β, MCP-1, and TNF-α) in the muscle tissues adjacent to joints in arthritic rats. These findings indicate that ME exerts protective effects against both systemic inflammation and the local inflammatory joint microenvironment, mirroring the immunomodulatory actions of biologic therapies such as tocilizumab (anti-IL-6R) and secukinumab (anti-IL-17A) [30,31]. Notably, ME's dual suppression of autoantibodies and cytokines positions it as a potential adjunct to conventional synthetic DMARDs or targeted synthetic DMARDs to enhance therapeutic efficacy. For instance, combin-

Table 3 Top 11 bioactive compounds identified in ME.

No.	CMAUP ID	Compound Name	Molecular Formula	PubChem CID	Bonding Energy (kcal·mol^{-1})
1	NPC484109	n.a.	$C_{28}H_{30}O_6$	n.a.	−7.8
2	NPC484108	n.a.	$C_{28}H_{30}O_6$	n.a.	−7.7
3	NPC39426	Genistein	$C_{15}H_{10}O_5$	5280961	−7.3
4	NPC129572	[(1R,2S)-1-hydroxy-1-(7-methoxy-2-oxochromen-8-yl)-3-methylbut-3-en-2-yl] 3-methylbutanoate	$C_{20}H_{24}O_6$	14779479	−6.7
5	NPC183864	Murrayone	$C_{15}H_{14}O_4$	5319964	−6.4
6	NPC2476	5-Demethylnobiletin	$C_{20}H_{20}O_8$	358832	−6.1
7	NPC85233	Nobiletin	$C_{21}H_{22}O_8$	72344	−6.1
8	NPC271600	7-Methoxy-8-[(1E)-3-oxobut-1-EN-1-YL]chromen-2-one	$C_{14}H_{12}O_4$	71434712	−6.1
9	NPC201547	3,5,6,7,8,3',4'-Heptamethoxyflavone	$C_{22}H_{24}O_9$	150893	−6.0
10	NPC294902	Caffeic Acid	$C_9H_8O_4$	689043	−5.9
11	NPC1075	cis-Caffeic acid	$C_9H_8O_4$	1549111	−5.4

ing ME with MTX may broaden cytokine coverage and reduce adverse reactions, as demonstrated in combination regimens involving *Tripterygium wilfordii* glycosides tablets [32]. Additionally, ME's inhibitory effect on NLRP3 aligns with emerging inflammasome-targeted strategies, suggesting potential compatibility with anakinra (an IL-1 receptor antagonist) or low-dose colchicine regimens [33, 34].

The dose-dependent suppression of FLS proliferation and migration, along with inhibition of MMP2/9 by ME extract, highlights its potential to mitigate joint destruction, a hallmark of RA progression. This mechanism parallels that of MMP inhibitors (e.g., doxycycline) and fibroblast-targeting therapies (e.g., rituximab in seropositive RA) [35, 36]. A secondary analysis of a randomized controlled trial demonstrated that MTX–doxycycline combination therapy more effectively reduced the Disease Activity Score 28 (DAS28) and serum inflammatory markers than MTX monotherapy, supporting the potential of ME in similar combinatorial approaches [37].

Oxidative stress, resulting from an imbalance between ROS production and antioxidant defenses, is a pivotal driver of RA progression [38]. ME's ability to restore redox balance, by reducing ROS and MDA levels while upregulating HO-1, NQO1, and SOD, addresses a critical gap in RA management. This antioxidant profile underscores ME's potential utility in refractory RA cases, where oxidative damage compromises conventional therapies, and highlights the promise of combining antioxidants with existing treatments to address unmet clinical needs, emphasizing the imperative for further mechanistic and translational research [39]. Additionally, ME's dual anti-inflammatory and anti-oxidative properties may offer therapeutic advantages for RA patients with cardiovascular comorbidities, given the established mechanistic links among chronic inflammation, oxidative stress, apoptosis, and myocardial dysfunction in RA [40].

Bioinformatic analysis provided further mechanistic insights, identifying the NF-κB signaling pathway as a central mediator of ME's effects. NF-κB comprises a family of widely expressed and inducible transcription factors, with the p65/p50 heterodimer being the most prevalent complex, primarily regulating inflammatory processes [41-44]. Overactivation of p65 and subsequent transactivation of effector molecules critically contribute to the progression of various chronic diseases, including RA [45, 46]. The AP-1 family consists of homo- and heterodimeric complexes, with the c-Fos/c-Jun heterodimer being the most prevalent and stable form, contributing to inflammation-associated diseases such as

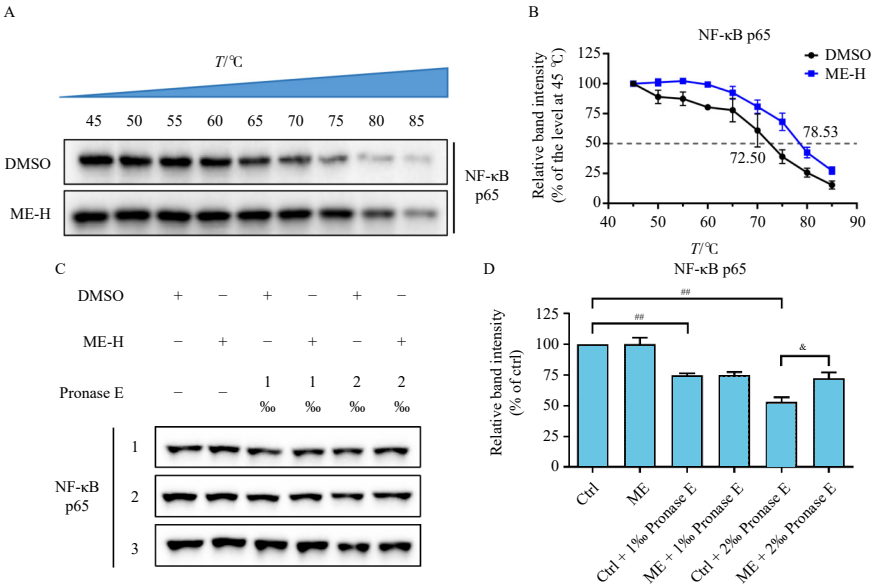

Fig. 9 ME demonstrated the capacity to target NF-κB p65. (A–B) Examination of the interaction between ME extract and the target protein p65 by CETSA (n = 3). (C–D) Determination of the interaction between ME extract and the target protein p65 by DARTS (n = 3). The results are presented as the mean ± SEM. $^{\#}P < 0.05$ and $^{\#\#}P < 0.01$ *vs* Ctrl; $^{\&}P < 0.05$ and $^{\&\&}P < 0.01$ *vs* Pronase E group.

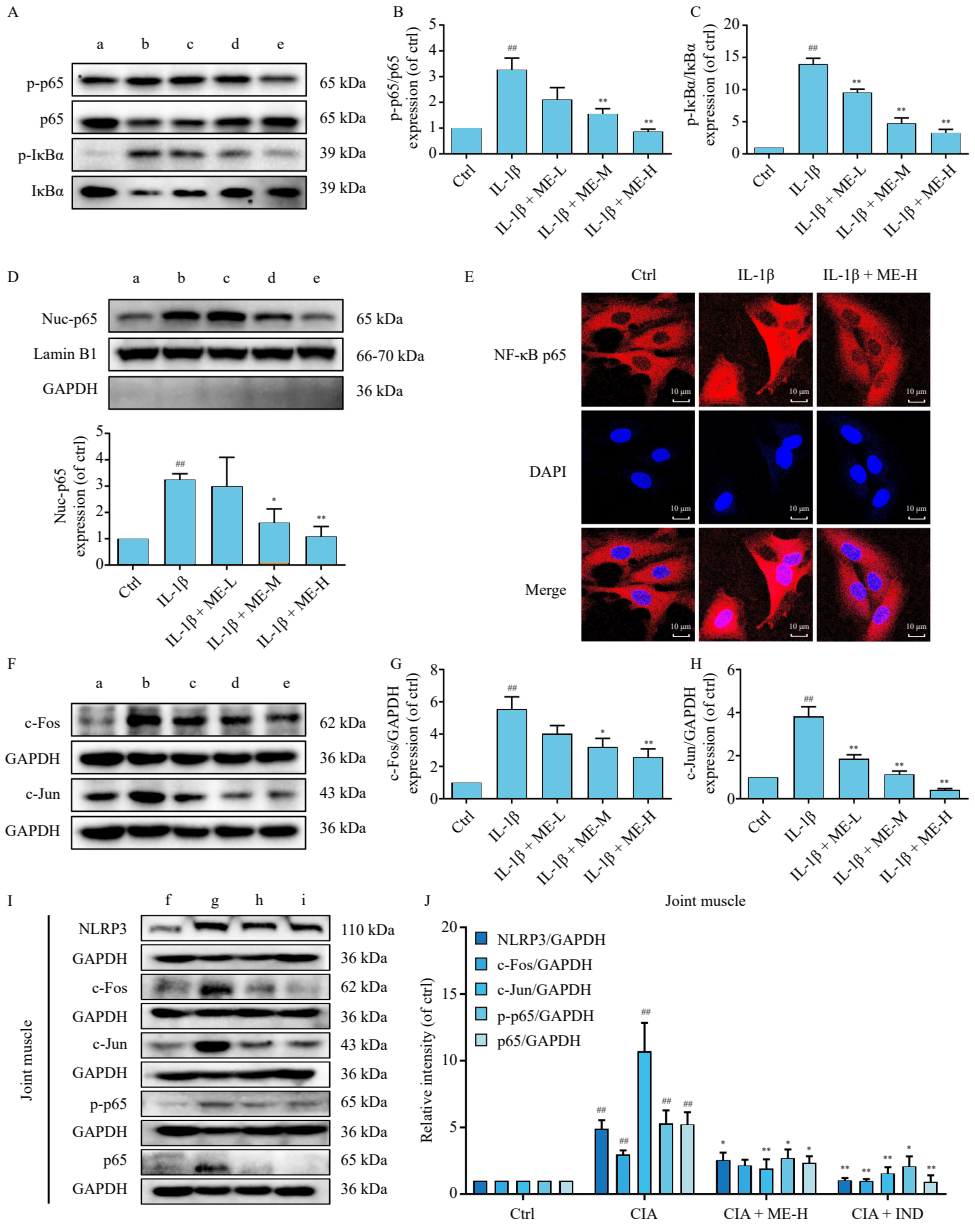

Fig. 10 Regulation of ME extract on NF-κB/AP-1 signaling pathways in IL-1β-triggered SW982 cells/CIA rats. (A–C) Suppression of the phosphorylation of p65 and IκBα in IL-1β-triggered SW982 cells by ME extract (n = 4). (D) Analysis of p65 expression in nuclear proteins using Western blotting (n = 3). (E) Assessment of p65 nuclear translocation through immunofluorescence staining. (F–H) Measurement of c-Jun and c-Fos expressions in IL-1β-triggered SW982 cells by Western blotting (n = 6). (I–J) Inhibition of NF-κB and AP-1 activation in CIA rats by ME extract (n = 6). The results are presented as the mean ± SEM. $^{\#}P < 0.05$ and $^{\#\#}P < 0.01$ *vs* Ctrl; $^{*}P<0.05$ and $^{**}P < 0.01$ *vs* IL-1β or CIA group. (a: Ctrl; b: IL-1β; c: IL-1β + ME-L; d: IL-1β + ME-M; e: IL-1β + ME-H; f: Ctrl; g: CIA; h: CIA + ME-H; i: CIA + IND).

RA [47, 48]. Pharmacological inhibition of NF-κB (using PDTC) and AP-1 (using SR11302) experimentally confirmed the dual regulatory roles of these pathways in mediating ME's anti-proliferative, anti-inflammatory, and anti-oxidative effects. Notably, ME's suppression of IκBα phosphorylation/degradation and p65 nuclear translocation aligns with the mechanisms of IκB kinase inhibitors (e.g., BMS-345541) and nuclear translocation inhibitors (e.g., JSH-23), while its modulation of AP-1 mirrors the action of T-5224 (a selective c-Fos/AP-1 inhibitor), thereby establishing a molecular foundation for ME's clinical translation in RA [49-51].

Collectively, ME extract emerges as a multitargeted therapeutic candidate for RA, combining anti-proliferative, anti-inflammatory, and anti-oxidative properties with a favorable safety profile. Its potential as a standalone or adjunct therapy may address unmet clinical needs in RA management, particularly in patients intolerant to conventional DMARDs or those exhibiting oxidative stress-driven pathogenesis. Future studies should prioritize pharmacokinetics, combination regimens, and biomarker validation to accelerate its integration into RA treatment paradigms.

5. Conclusions

In CIA rats, ME alleviated clinical symptoms, attenuated histopathological joint damage, including synovial hyperplasia, cartilage degeneration, and bone erosion, ameliorated inflammation, and reduced oxidative stress. In IL-1β-stimulated SW982 synoviocytes, ME inhibited proliferation and migration, suppressed the inflammatory response, and mitigated oxidative stress. The use of PDTC and SR11302 further corroborated the involvement of the NF-κB and AP-1 pathways in mediating ME's anti-proliferative, anti-inflammatory, and anti-oxidative effects in RA. These multidimensional findings not only elucidate the anti-arthritic mechanisms of ME, which involve crosstalk among proliferation, inflammation, and oxidative stress, but also underscore its translational potential as a multi-target phytomedicine, offering novel insights for the development of plant-derived therapies against

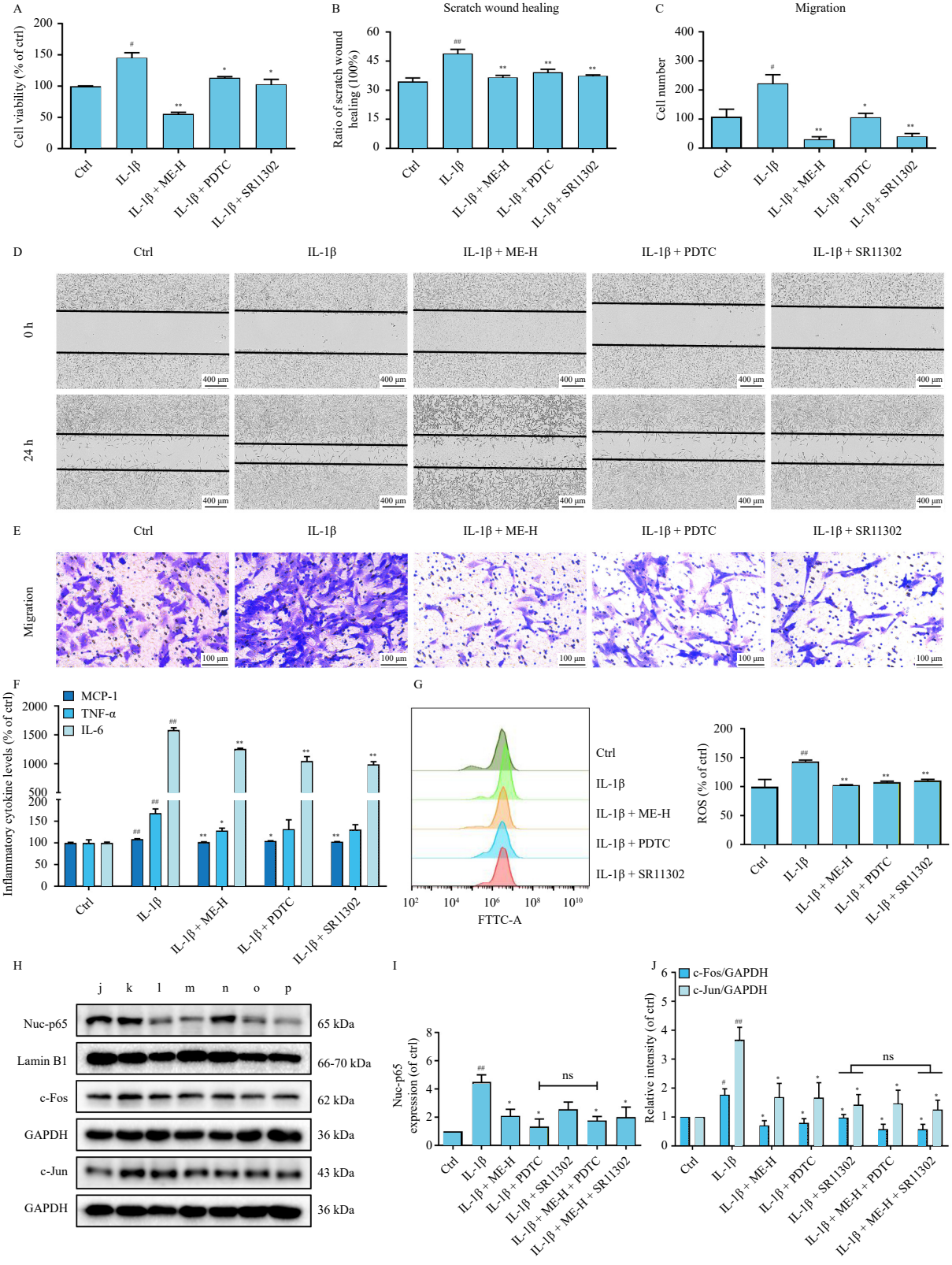

Fig. 11 NF-κB/AP-1 pathway modulation underpinned ME's anti-proliferative, anti-inflammatory, and anti-oxidative effects. (A) Suppression of IL-1β-triggered proliferation by ME extract/PDTC/SR11302 (n = 4). (B–E) Inhibition of IL-1β-triggered migration by ME extract/PDTC/SR11302 (n = 3). (F) Detection of MCP-1, TNF-α, and IL-6 in the culture supernatants of IL-1β-triggered SW982 cells by ELISA (n = 3). (G) Determination of ROS levels in IL-1β-triggered SW982 cells by flow cytometry (n = 4). (H–J) Measurement of nuc-p65, c-Fos, and c-Jun expressions in IL-1β-triggered SW982 cells by Western blotting (n = 3). The results are presented as the mean ± SEM. $^{\#}P < 0.05$ and $^{\#\#}P < 0.01$ *vs* Ctrl; $^{*}P < 0.05$ and $^{**}P < 0.01$ *vs* IL-1β group. (j: Ctrl; k: IL-1β; l: IL-1β + ME-H; m: IL-1β + PDTC; n: IL-1β + SR11302; o: IL-1β + ME-H + PDTC; p: IL-1β + ME-H + SR11302; ns: no significance).

autoimmune arthritis. Furthermore, the integration of bioinformatic analysis with experimental validation highlights the critical role of systems biology in deciphering complex drug–disease interactions.

Funding

This work was supported by the Science and Technology Development Fund of Macau SAR (Nos. 0159/2020/A3, 0212/

2024/AGJ, 0002/2025/NRP), the Research Committee of the University of Macau (Nos. MYRG2022-00189-ICMS, MYRG-GRG2023-00214-ICMS-UMDF, MYRG-GRG2024-00240-ICMS-UMDF), and the Innovation Team and Talents Cultivation Program of National Administration of Traditional Chinese Medicine (No. ZYYCXTD-D-202005).

Declaration of competing interests

These authors have no conflict of interest to declare.

References

1 Sparks JA. Rheumatoid arthritis. *Ann Intern Med*. 2019;170(1):ITC1-ITC16. https://doi.org/10.7326/AITC201901010.
2 Zhang C, Weng Y, Wang H, et al. A synergistic effect of triptolide and curcumin on rheumatoid arthritis by improving cell proliferation and inducing cell apoptosis *via* inhibition of the IL-17/NF-κB signaling pathway. Int Immunopharmacol. 2024;142(Pt A):112953. https://doi.org/10.1016/j.intimp.2024.112953 .
3 Aletaha D, Smolen JS. Diagnosis and management of rheumatoid arthritis: a review. *JAMA*. 2018;320(13):1360-1372. https://doi.org/10.1001/jama.2018.13103.
4 Zhang Y, Yu X, Zhou C, et al. Targeting cellular senescence in senile osteoporosis: therapeutic potential of traditional Chinese medicine. *Front Med (Lausanne)*. 2023;10:1288993. https://doi.org/10.3389/fmed.2023.1288993.
5 Zhao M, Xiao L, Linghu KG, et al. Comprehensive comparison on the anti-inflammation and GC-MS-based metabolomics discrimination between *Bupleuri chinense* DC. and B. scorzonerifolium Willd . *Front Pharmacol*. 2022;13:1005011. https://doi.org/10.3389/fphar.2022.1005011.
6 Lu M, Du Z, Yuan S, et al. Comparison of the preventive effects of *Murraya exotica* and *Murraya paniculata* on alcohol-induced gastric lesions by pharmacodynamics and metabolomics. *J Ethnopharmacol*. 2021;281:114567. https://doi.org/10.1016/j.jep.2021.114567.
7 Qi Y, Wang L, Wang N, et al. A comprehensive review of the botany, phytochemistry, pharmacology, and toxicology of Murrayae Folium et Cacumen. *Front Pharmacol*. 2024;15:1337161. https://doi.org/10.3389/fphar.2024.1337161.
8 Liang H, Shi Y, Zeng K, et al. Coumarin derivatives from the leaves and twigs of *Murraya exotica* L. and their anti-inflammatory activities . *Phytochemistry*. 2020;177:112416. https://doi.org/10.1016/j.phytochem.2020.112416.
9 Xu G, Feng L, Song P, et al. Isomeranzin suppresses inflammation by inhibiting M1 macrophage polarization through the NF-κB and ERK pathway. *Int Immunopharmacol*. 2016;38:175-185. https://doi.org/10.1016/j.intimp.2016.05.027.
10 Huang J, Ren Q, Jiao L, et al. TMF suppresses chondrocyte hypertrophy in osteoarthritic cartilage by mediating the FOXO3a/BMPER pathway. *Exp Ther Med*. 2024;28(1):283. https://doi.org/10.3892/etm.2024.12571.
11 Scherer HU, Häupl T, Burmester GR. The etiology of rheumatoid arthritis. *J Autoimmun*. 2020;110:102400. https://doi.org/10.1016/j.jaut.2019.102400.
12 Li D, Liu W, Sun S, et al. Chinese herbal formula, modified Xianfang Huoming Yin, alleviates the inflammatory proliferation of rat synoviocytes induced by IL-1β through regulating the migration and differentiation of T lymphocytes. *J Ethnopharmacol*. 2023;309:116297. https://doi.org/10.1016/j.jep.2023.116297.
13 Ma QS, Linghu KG, Zhang T, et al. *Sigesbeckia glabrescens* Makino extract attenuated the collagen-induced arthritis through inhibiting the synovial hyperplasia and inflammation. *Chin Med*. 2020;15:91. https://doi.org/10.1186/s13020-020-00372-4 .
14 Lee S, Choi E, Chae S, et al. Identification of MYH9 as a key regulator for synoviocyte migration and invasion through secretome profiling. *Ann Rheum Dis*. 2023;82(8):1035-1048. https://doi.org/10.1136/ard-2022-223625.
15 Ichise Y, Saegusa J, Tanaka-Natsui S, et al. Soluble CD14 induces pro-inflammatory cytokines in rheumatoid arthritis fibroblast-like synovial cells *via* Toll-like receptor 4. *Cells*. 2020;9(7):1689. https://doi.org/10.3390/cells9071689.
16 Lee HR, Yoo SJ, Kim J, et al. LKB1 regulates inflammation of fibroblast-like synoviocytes from patients with rheumatoid arthritis *via* AMPK-dependent SLC7A11-NOX4-ROS signaling. *Cells*. 2023;12(9):1263. https://doi.org/10.3390/cells12091263.
17 Sun Y, Liu J, Wen J, et al. Overexpression of long noncoding RNA LINC00638 inhibits inflammation and oxidative stress in rheumatoid arthritis fibroblast-like synoviocytes by regulating the Nrf2/HO-1 pathway. *Immun Inflamm Dis*. 2022;10(7):e663. https://doi.org/10.1002/iid3.663.
18 Sims NA, Green JR, Glatt M, et al. Targeting osteoclasts with zoledronic acid prevents bone destruction in collagen-induced arthritis. *Arthritis Rheum*. 2004;50(7):2338-2346. https://doi.org/10.1002/art.20382.
19 Linghu KG, Xiong SH, Zhao GD, et al. *Sigesbeckia orientalis* L. extract alleviated the collagen Type II-induced arthritis through inhibiting multi-target-mediated synovial hyperplasia and inflammation. Front Pharmacol. 2020;11:547913. https://doi.org/10.3389/fphar.2020.547913 .
20 Arnott JA, Planey SL. The influence of lipophilicity in drug discovery and design. *Expert Opin Drug Discov*. 2012;7(10):863-875. https://doi.org/10.1517/17460441.2012.714363.
21 Daina A, Michielin O, Zoete V. SwissADME: a free web tool to evaluate pharmacokinetics, drug-likeness and medicinal chemistry friendliness of small molecules. *Sci Rep*. 2017;7:42717. https://doi.org/10.1038/srep42717.
22 Daina A, Michielin O, Zoete V. SwissTargetPrediction: updated data and new features for efficient prediction of protein targets of small molecules. *Nucleic Acids Res*. 2019;47(W1):W357-W364. https://doi.org/10.1093/nar/gkz382.
23 Linghu KG, Ma QS, Zhao GD, et al. Leocarpinolide B attenuates LPS-induced inflammation on RAW264.7 macrophages by mediating NF-κB and Nrf2 pathways . *Eur J Pharmacol*. 2020;868:172854. https://doi.org/10.1016/j.ejphar.2019.172854.
24 Ren YS, Li HL, Piao XH, et al. Drug affinity responsive target stability (DARTS) accelerated small molecules target discovery: principles and application. *Biochem Pharmacol*. 2021;194:114798. https://doi.org/10.1016/j.bcp.2021.114798.
25 Meng M, Wang L, Yao Y, et al. *Ganoderma lucidum* polysaccharide peptide (GLPP) attenuates rheumatic arthritis in rats through inactivating NF-κB and MAPK signaling pathways. *Phytomedicine*. 2023;119:155010. https://doi.org/10.1016/j.phymed.2023.155010 .
26 Mititelu RR, Pădureanu R, Băcănoiu M, et al. Inflammatory and oxidative stress markers–mirror tools in rheumatoid arthritis. *Biomedicines*. 2020;8(5):125. https://doi.org/10.3390/biomedicines8050125.
27 Shahbazi K, Raeeszadeh M, Akradi L. The effectiveness of levamisole and broccoli in lead poisoning: hematobiochemical changes and tissue damage in the liver, kidney, and spleen of Wistar rats. *J Toxicol*. 2024;2024:8283897. https://doi.org/10.1155/jt/2024/8283897.
28 Fraser SD, Lin SX, Stammers M, et al. Persistently normal blood tests in patients taking methotrexate for RA or azathioprine for IBD: a retrospective cohort study. *Br J Gen Pract*. 2022;72(720):e528-e537. https://doi.org/10.3399/BJGP.2021.0595.
29 Breedveld AC, van Gool MMJ, van Delft MAM, et al. IgA immune complexes induce osteoclast-mediated bone resorption. *Front Immunol*. 2021;12:651049. https://doi.org/10.3389/fimmu.2021.651049.
30 Fa'ak F, Buni M, Falohun A, et al. Selective immune suppression using interleukin-6 receptor inhibitors for management of immune-related adverse events. *J Immunother Cancer*. 2023;11(6):e006814. https://doi.org/10.1136/jitc-2023-006814.
31 Donzella D, Bellis E, Campisi P, et al. New onset sarcoidosis following biologic treatment in patients with seronegative inflammatory arthritis: a case series and systematic literature review. *Autoimmun Rev*. 2024;23(3):103481. https://doi.org/10.1016/j.autrev.2023.103481.
32 Shu H, Chen XY, Zhao J, et al. Efficacy and safety of *Tripterygium wilfordii* glycosides tablets combined with Western medicine for patients with rheumatic immune diseases. *World J Clin Cases*. 2025;13(6):95513. https://doi.org/10.12998/wjcc.v13.i6.95513.
33 Hurtado-Navarro L, Cuenca-Zamora EJ, Zamora L, et al. NLRP3 inflammasome activation and symptom burden in KRAS-mutated CMML patients is reverted by IL-1 blocking therapy. *Cell Rep Med*. 2023;4(12):101329. https://doi.org/10.1016/j.xcrm.2023.101329.
34 Lin N, Dai Q, Zhang Y, et al. Chinese classical decoction Wuwei Xiaodu Drink alleviates gout arthritis by suppressing NLRP3-Mediated inflammation. *Front Pharmacol*. 2024;15:1388753. https://doi.org/10.3389/fphar.2024.1388753.
35 Radić M, Belančić A, Đogaš H, et al. Tetracyclines in rheumatoid arthritis: dual anti-inflammatory and immunomodulatory roles, effectiveness, and safety insights. *Antibiotics (Basel)*. 2025;14(1):65. https://doi.org/10.3390/antibiotics14010065.
36 Jeong S, Choi S, Park SM, et al. Incident and recurrent herpes zoster for first-line bDMARD and tsDMARD users in seropositive rheumatoid arthritis patients: a nationwide cohort study. *Arthritis Res Ther*. 2022;24(1):180. https://doi.org/10.1186/s13075-022-02871-1.
37 Ibrahem EM, El-Gendi SS, Mahmoud AA, et al. Predictors of cardiovascular affection in patients with active rheumatoid arthritis: secondary analysis of a randomized controlled trial. *Curr Rheumatol Rev*. 2021;17(2):258-266. https://doi.org/10.2174/1573397116666201113090145.
38 Han Z, Gao X, Wang Y, et al. Ultrasmall iron-quercetin metal natural product nanocomplex with antioxidant and macrophage regulation in rheumatoid arthritis. *Acta Pharm Sin B*. 2023;13(4):1726-1739. https://doi.org/10.1016/j.apsb.2022.11.020.
39 Bilski R, Nuszkiewicz J. Antioxidant therapies as emerging adjuncts in rheumatoid arthritis: targeting oxidative stress to enhance treatment outcomes. *Int J Mol Sci*. 2025;26(7):2873. https://doi.org/10.3390/ijms26072873.
40 Lazou A, Ikonomidis I, Bartekova M, et al. Chronic inflammatory diseases, myocardial function and cardioprotection. *Br J Pharmacol*. 2020;177(23):5357-5374. https://doi.org/10.1111/bph.14975.
41 Zhang J, Zhang M, Huo XK, et al. Macrophage inactivation by small molecule wedelolactone *via* targeting sEH for the treatment of LPS-induced acute lung injury. *ACS Cent Sci*. 2023;9(3):440-456. https://doi.org/10.1021/acscentsci.2c01424.
42 Sun CP, Zhou JJ, Yu ZL, et al. Kurarinone alleviated Parkinson's disease *via* stabilization of epoxyeicosatrienoic acids in animal model. *Proc Natl Acad Sci U S A*. 2022;119(9):e2118818119. https://doi.org/10.1073/pnas.2118818119.
43 Zhang J, Luan ZL, Huo XK, et al. Direct targeting of sEH with alisol B alleviated the apoptosis, inflammation, and oxidative stress in cisplatin-induced acute kidney injury. *Int J Biol Sci*. 2023;19(1):294-310. https://doi.org/10.7150/ijbs.78097.
44 Zhang J, Zhang WH, Morisseau C, et al. Genetic deletion or pharmacological inhibition of soluble epoxide hydrolase attenuated particulate matter 25 exposure mediated lung injury . *J Hazard Mater*. 2023;458:131890. https://doi.org/10.1016/j.jhazmat.2023.131890.
45 Jimi E, Fei H, Nakatomi C. NF-κB signaling regulates physiological and pathological chondrogenesis. *Int J Mol Sci*. 2019;20(24):6275. https://doi.org/10.3390/ijms20246275.
46 Jia YX, Wang N, Hui SW, et al. Discovery of soluble epoxide hydrolase inhibitors from *Inula britannica*: inhibition kinetics, molecular dynamics simulation, biochemical, and *in vitro* cell-based studies. *Int J Biol Macromol*. 2025;306(Pt 3):141704. https://doi.org/10.1016/j.ijbiomac.2025.141704 .
47 Hannemann N, Jordan J, Paul S, et al. The AP-1 transcription factor c-Jun promotes arthritis by regulating cyclooxygenase-2 and arginase-1 expression in macrophages. *J Immunol*. 2017;198(9):3605-3614. https://doi.org/10.4049/jimmunol.1601330.
48 Zhang HL, Wang N, Shi XL, et al. Sesquiterpenoids from *Inula britannica* and their potential mechanism for immunomodulation. *Phytochemistry*. 2025;231:114343. https://doi.org/10.1016/j.phytochem.2024.114343.
49 Sahu N, Grandi FC, Bhutani N. A single-cell mass cytometry platform to map the effects of preclinical drugs on cartilage homeostasis. *JCI Insight*. 2022;7(20):e160702. https://doi.org/10.1172/jci.insight.160702.
50 Chen Y, Tian Y, Liu H, et al. Repurposed drug agomelatine is therapeutic against collagen-induced arthritis *via* iNOS targeting. *Int Immunopharmacol*. 2024;130:111750. https://doi.org/10.1016/j.intimp.2024.111750.
51 Motomura H, Seki S, Shiozawa S, et al. A selective c-Fos/AP-1 inhibitor prevents cartilage destruction and subsequent osteophyte formation. *Biochem Biophys Res Commun*. 2018;497(2):756-761. https://doi.org/10.1016/j.bbrc.2018.02.147.